Reconstructing network topology and coupling strengths in directed networks of discrete-time dynamics

Pik-Yin Lai*

Department of Physics and Center for Complex Systems, National Central University, Chung-Li District, Taoyuan City 320, Taiwan, Republic of China

(Received 10 October 2016; revised manuscript received 26 December 2016; published 24 February 2017)

Reconstructing network connection topology and interaction strengths solely from measurement of the dynamics of the nodes is a challenging inverse problem of broad applicability in various areas of science and engineering. For a discrete-time step network under noises whose noise-free dynamics is stationary, we derive general analytic results relating the weighted connection matrix of the network to the correlation functions obtained from time-series measurements of the nodes for networks with one-dimensional intrinsic node dynamics. Information about the intrinsic node dynamics and the noise strengths acting on the nodes can also be obtained. Based on these results, we develop a scheme that can reconstruct the above information of the network using only the time-series measurements of node dynamics as input. Reconstruction formulas for higher-dimensional node dynamics are also derived and illustrated with a two-dimensional node dynamics network system. Furthermore, we extend our results and obtain a reconstruction scheme even for the cases when the noise-free dynamics is periodic. We demonstrate that our method can give accurate reconstruction results for weighted directed networks with linear or nonlinear node dynamics of various connection topologies, and with linear or nonlinear couplings.

DOI: 10.1103/PhysRevE.95.022311

I. INTRODUCTION

Since the emergence of the "big data" era [1], in which there are huge amounts of dynamical data to be mined in many different disciplines, there has been a need for novel and reliable methods of network reconstruction [2,3] that can provide insight and advance the fundamental understanding of these systems, which would otherwise be buried in these massive amounts of data. Many systems of interest in physics, biology, or social sciences are multicomponent systems in which the components or nodes interact with each other. Examples include weather and atmospheric data, financial time-series, power grid networks, communication and web networks, and social networks [4–6]. Other complex biological networks of interest are gene expression data for gene regulatory networks [7,8], multielectrode array measurements for neuronal networks and functional MRI measurements for the brain network [9], disease infection networks, etc. Despite the vast amount of data, it remains a big challenge to utilize the experimental measurements to provide in-depth theoretical insights into these systems. One of the major goals in bridging the experimental data and a theoretical understanding in a complex interacting system is to provide a solution to the following crucial inverse problem: how can we decipher the wiring diagram and reconstruct the underlying network and intrinsic dynamics of the nodes from measurements and observations [2,10,11]? An accurate solution to the above network reconstruction problem can provide new insights and breakthroughs in the fundamental mechanisms behind many complex phenomena. We would also like to stress that one should aim for a model-free method (i.e., one in which no prior knowledge about the details of the node dynamics and the coupling functional form is needed), and there should be no information required other than the nodal dynamics of a complex interacting network. For example, we do not need other information such as the nodal dynamics or the responses of the systems upon perturbations as in previous studies [12–16]. The data of the system dynamics, passively recorded and observed, are sufficient for practical applications. Successful methods for uncovering knowledge from data should be very general and can be widely applicable to various areas in physics, biology, and many disciplines in science, and they will allow for a deep and broad impact.

The most important feature of a complex network is how the nodes are connected, including the strength of the connection and their directionality. This feature determines the overall properties and governs the dynamics and functionality of the network. However, such wiring information of a network is often not directly measurable, and thus the network reconstruction is crucial in providing significant insights and understanding of the fundamental mechanism behind the overall behavior of the systems. Recently, there have been a few attempts [17–20] aiming to uncover the connectivity, directions, and coupling strengths of a network described by continuous-time coupled ordinary differential equations. On the other hand, there is a large class of systems in nature whose dynamics are described by discrete-time steps, constituting networks with discrete-time dynamics. Often these discrete-time dynamical systems, such as coupled map networks [21], display even richer collective dynamical behavior. Based on the ideas [17,18,22] that noise can reveal the interactions between nodes in the dynamical data of the network, in this paper we will present our approach to the challenging inverse problem of network reconstruction solely from the measurement of dynamical time-series data. In particular, we focus on network dynamics with discrete-time steps, and we derive reconstruction formulas for directed networks in the presence of white noise. We establish reconstruction formulas for one- and higher-dimensional intrinsic node dynamics. Our method works well for network dynamics fluctuating around the noise-free stationary state, and we also derive the reconstruction

*pylai@phy.ncu.edu.tw

scheme for dynamics that fluctuates around the periodic state. All of these reconstruction schemes are well verified explicitly by numerically generated dynamics of known connections, intrinsic node dynamics, noise strengths, different linear and nonlinear coupling functions, and various network topologies.

II. COUPLED MAP NETWORK UNDER NOISES

Consider a network with N nodes whose intrinsic one-dimensional dynamics of the ith node at discrete-time step n, $x_i(n)$, is described by the nonlinear function $f_i(x_i)$. Nodes i and j are connected by directed and weighted links given by the matrix $\mathbf{W}$. The dynamics is governed by

$$x_i(n+1) = f_i(x_i(n)) + \sum_{j\neq i}^{N} W_{ij} h(x_i(n), x_j(n)) + \eta_i(n), \tag{1}$$

where η_i is a zero-mean Gaussian white noise that acts on the node i. In many situations, the weighted matrix takes the form $W_{ij} = g_{ij}A_{ij}$, with the adjacency matrix of elements $A_{ij} = 0$ or 1, and connection weights g_{ij}. h is some coupling function describing the interaction between nodes i and j. Furthermore, we assume that in the presence of noises, the system approaches some asymptotic dynamics and $x_i(n)$ fluctuates around the noise-free solution $X_i(n)$.

Considering a small deviation from the noise-free solution, $y_i(n) \equiv x_i(n) - X_i(n)$, and keeping to linear order in y_i, one has for $i = 1,2,\ldots,N$,

$$\begin{aligned} y_i(n+1) \simeq\ & f_i'(X_i) y_i(n) + \sum_{j=1}^{N} [W_{ij}\partial_2 h(X_i, X_j) y_j(n) \\ & + W_{ij}\partial_1 h(X_i, X_j) y_i(n)] + \eta_i(n), \end{aligned} \tag{2}$$

where $\partial_1 h$ and $\partial_2 h$ denote the derivatives with respect to the first and second variables in h, respectively. Equation (2) can be written as

$$\vec{y}(n+1) \simeq \mathbf{N}\vec{y}(n) + \vec{\eta}(n), \tag{3}$$

where the matrix elements of $\mathbf{N}$ are given by

$$\begin{aligned} N_{ij} =\ & W_{ij}\partial_2 h(X_i, X_j) \\ & + \left[f_i'(X_i) + \sum_m W_{im}\partial_1 h(X_i, X_m) \right] \delta_{ij}. \end{aligned} \tag{4}$$

In the next section, we first consider the case in which the noise-free solution is time-independent, i.e., $x_i(n)$ fluctuates about the time-dependent X_i, and hence $\mathbf{N}$ is time-independent. Equation (3) can be solved to give

$$\vec{y}(n) \simeq \mathbf{N}^n \vec{y}(0) + \sum_{k=0}^{n-1} \mathbf{N}^{n-k-1} \vec{\eta}(k). \tag{5}$$

The white noise has zero mean with variance given by the noise correlation matrix $\boldsymbol{\sigma}$:

$$\overline{\vec{\eta}(n)\vec{\eta}^{\mathsf{T}}(n')} = \boldsymbol{\sigma}\delta_{nn'}, \quad \overline{\vec{\eta}(n)} = 0, \tag{6}$$

where the $\overline{\cdots}$ stands for ensemble average over the noise, which can be obtained in practice by a time average over the asymptotic dynamics over an extended period of time, $\langle\cdots\rangle$.

We aim to extract the elements of the (asymmetric) coupling matrix W_{ij}, the information on the noises, and the intrinsic dynamics [such as $f_i'(X_i)$] using only the measured time series $x_i(t)$ as input. It will be shown that this can be achieved by computing the time-lagged correlation matrices $\mathbf{K}_\tau$ (where $\tau = 0,1,2,\ldots$ is the forward time lags) defined as follows:

$$\mathbf{K}_\tau = \langle \vec{y}(n+\tau)\vec{y}^{\mathsf{T}}(n) \rangle. \tag{7}$$

In practice, the time-average $\langle\cdots\rangle$ is performed over some finite-time duration $T_{\rm av}$ of measurements. We first show that there are exact relations between the matrices $\mathbf{N}$ (and hence $\mathbf{W}$), $\mathbf{K}_\tau$, and $\boldsymbol{\sigma}$.

III. RECONSTRUCTION FORMULAS FOR A COUPLED MAP NETWORK UNDER WHITE NOISES

The uncorrelated white noise η has a zero mean with variance given by $\langle \eta_i(n)\eta_j(n') \rangle = \sigma_{ij}\delta_{nn'}$, where σ_{ij} are the noise correlation matrix elements, and the noise strength at node i is given by the variance σ_{ii}. We first derive an exact relation between the time-lag covariance matrices. Using (3), one has

$$\begin{aligned} \mathbf{K}_{\tau+1} &= \langle \vec{y}(n+\tau+1)\vec{y}^{\mathsf{T}}(n) \rangle && (8)\\ &= \langle \mathbf{N}\vec{y}(n+\tau)\vec{y}^{\mathsf{T}}(n) \rangle + \langle \vec{\eta}(n)\vec{y}^{\mathsf{T}}(n) \rangle && (9)\\ &= \mathbf{N}\mathbf{K}_\tau, && (10) \end{aligned}$$

where $\langle \vec{\eta}(n)\vec{y}^{\mathsf{T}}(n) \rangle = 0$, which follows from the white noise nature of $\vec{\eta}$ and from (5) that $\vec{y}(n)$ depends only on noises at earlier times. Similarly, one has

$$\begin{aligned} \mathbf{K}_0 &= \langle \vec{y}(n)\vec{y}^{\mathsf{T}}(n) \rangle && (11)\\ &= \langle \mathbf{N}\vec{y}(n)[\mathbf{N}\vec{y}(n)]^{\mathsf{T}} \rangle + \langle \vec{\eta}(n)\vec{\eta}^{\mathsf{T}}(n) \rangle && (12)\\ &= \mathbf{N}\mathbf{K}_0\mathbf{N}^{\mathsf{T}} + \boldsymbol{\sigma}. && (13) \end{aligned}$$

Finally, one obtains the reconstruction formulas for the coupling and noise matrices:

$$\mathbf{N} = \mathbf{K}_1\mathbf{K}_0^{-1} = \mathbf{K}_2\mathbf{K}_1^{-1} = \cdots \mathbf{K}_\tau\mathbf{K}_{\tau-1}^{-1}, \tag{14}$$

$$\boldsymbol{\sigma} = \mathbf{K}_0 - \mathbf{N}\mathbf{K}_0\mathbf{N}^{\mathsf{T}} = \mathbf{K}_0 - \mathbf{K}_1\mathbf{K}_0^{-1}\mathbf{K}_1^{\mathsf{T}}. \tag{15}$$

Hereafter, the coupling function h is taken to be of the form $h(x_1,x_2) = h(x_2 - x_1)$ and $h(-z) = -h(z)$ [hence $h'(0) > 0$], which tends to synchronize the dynamics of the nodes. Thus $\partial_2 h = h'(0) = -\partial_1 h$ in Eq. (4), and

$$N_{ij} = \left(f_i' - h' \sum_m W_{im} \right) \delta_{ij} + h' W_{ij}. \tag{16}$$

For notational simplicity, we denoted $h' \equiv h'(0)$ and $f_i' \equiv f_i'(X_i)$ in the above and throughout the paper. Approximate the ensemble average by an average over a finite averaging time $T_{\rm av}$, one can compute the correlation matrices from the time-series data. In practice, the noise-free solution can be approximated by $X_i \simeq \langle x_i \rangle$. Also, short time-lag covariance matrices can be measured more accurately than large τ ones, thus it suffices to measure and use $\mathbf{K}_0$ and $\mathbf{K}_1$ for network reconstructions.

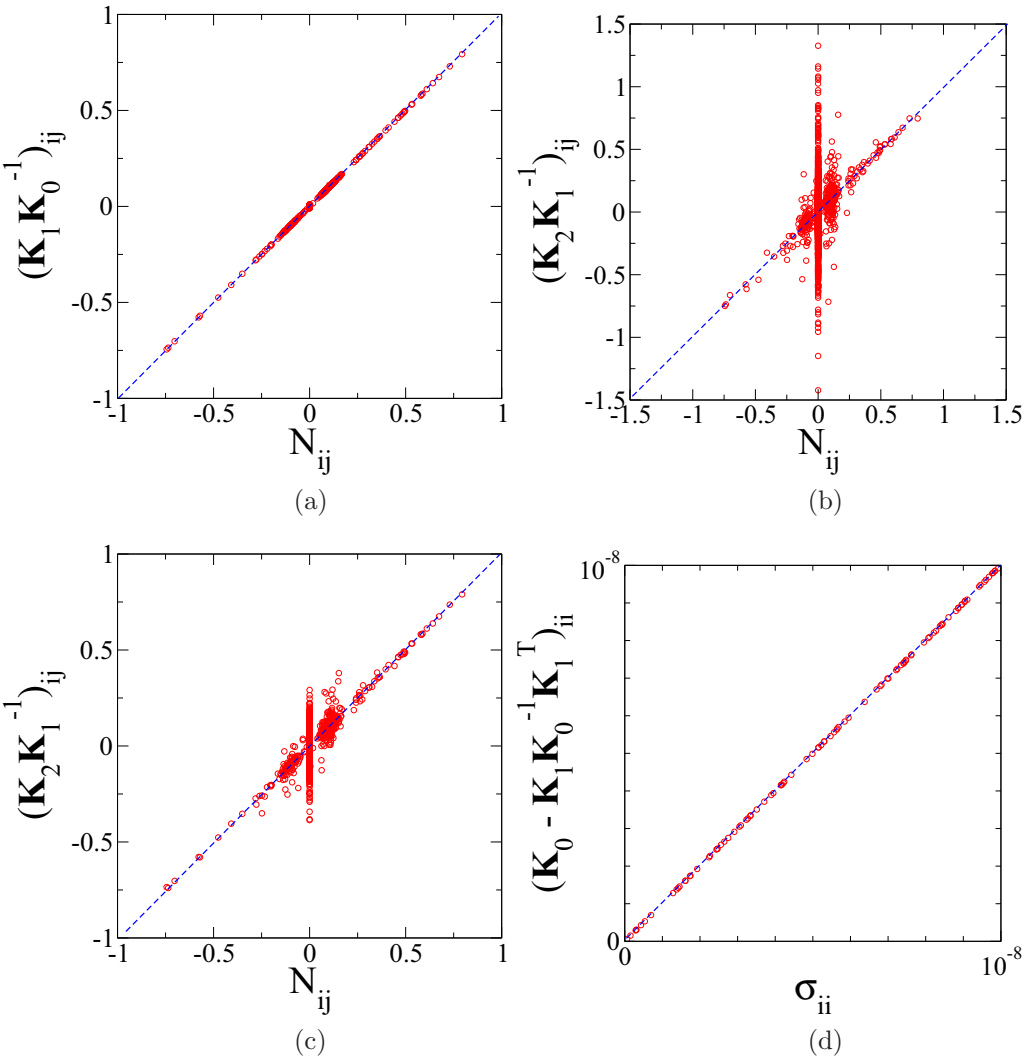

FIG. 1. Verification of the reconstruction formulas for the directed weighted random network. Heterogeneous coupled Logistic map dynamics $f_i(x) = r_i x(1-x)$ with r_i uniformly distributed in (0,0.8] and linear couplings. (a) $(\mathbf{K}_1\mathbf{K}_0^{-1})_{ij}$. (b) $(\mathbf{K}_2\mathbf{K}_1^{-1})_{ij}$ vs the actual N_{ij}, verifying (14). $T_{\rm av} = 10^6$. (c) $(\mathbf{K}_2\mathbf{K}_1^{-1})_{ij}$ vs the actual N_{ij}, with $T_{\rm av} = 7\times10^6$. (d) $(\mathbf{K}_0 - \mathbf{K}_1\mathbf{K}_0^{-1}\mathbf{K}_1^{\intercal})_{ii}$ vs the actual σ_{ii}, verifying (15). $T_{\rm av} = 10^6$.

A. Network reconstruction performances: Numerical results

To verify our main results and evaluate the effectiveness of the reconstruction method, we numerically generate the dynamics of networks of given W_{ij} with various nonlinear intrinsic dynamics and linear and nonlinear couplings, and we compare the known weighted asymmetric matrix with that of the reconstructed one using Eqs. (17) and (18) below. We test our method using weighted random (WR) networks [23,24]. Weighted random networks with $N = 100$ nodes are generated with a connection probability p and coupling strengths of each link taken from a distribution of two Gaussians with means 0.1 and -0.1 (with relative fraction of 0.8 and 0.2, respectively), and standard deviations 0.02. WR1 are Erdös-Rényi random networks [23] generated with connection probability p ($p = 0.05$ unless otherwise stated). WR3 is a random network with three disconnect parts each with (almost) the same number of nodes, and the total number of links in the entire network is the same as that of WR1. In addition to logistic dynamics [25], we also study the nonlinear intrinsic dynamics given by the cubic map and Hill form. Care has been taken to choose parameters such that the resulting asymptotic dynamics remains bounded. Unless otherwise stated, we take the white noise matrix to be diagonal with strengths σ_{ii} uniformly distributed in the interval $(0, 10^{-8}]$. Figures 1(a) and 1(b) show the plots of the computed matrix elements of $\mathbf{K}_1\mathbf{K}_0^{-1}$ and $\mathbf{K}_2\mathbf{K}_1^{-1}$ versus the matrix elements of $\mathbf{N}$ verifying (14). Note that the reconstruction formula holds very well for $\mathbf{K}_1\mathbf{K}_0^{-1}$ and less satisfactorily for $\mathbf{K}_2\mathbf{K}_1^{-1}$, but it can be improved if $T_{\rm av}$ is increased [see Fig. 1(c)]. Figure 1(d) verifies that the noise reconstruction formula for $\boldsymbol{\sigma}$ in Eq. (15) holds very well.

Using the first part of (14), one can reconstruct the coupling matrix W_{ij} and f_i' via

$$h' W_{ij} = \sum_m (\mathbf{K}_1)_{im} \left(\mathbf{K}_0^{-1}\right)_{mj} \quad \text{for } i \neq j, \quad W_{ii} = 0, \tag{17}$$

$$f_i' = \sum_m (\mathbf{K}_1)_{im} \left(\mathbf{K}_0^{-1}\right)_{mi} + \sum_{k\neq i} \sum_m (\mathbf{K_1})_{im} \left(\mathbf{K_0}^{-1}\right)_{mk}. \tag{18}$$

One can further improve the reconstruction accuracy by first extracting the adjacency matrix, i.e., identifying the

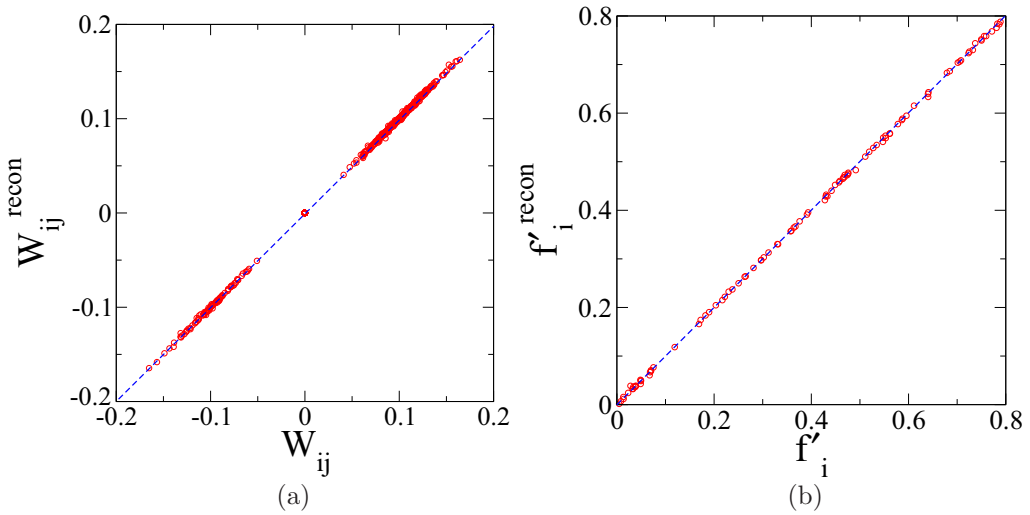

FIG. 2. Reconstruction for a directed weighted random network with heterogeneous coupled logistic map dynamics $f_i(x) = r_i x(1-x)$ and linear couplings as in Fig. 1. $T_{\rm av} = 10^6$. (a) Reconstructed W_{ij} using (17) vs the actual W_{ij}. (b) The reconstructed f_i' using (18) vs the actual f_i'.

unconnected node pairs. This can be achieved by noticing for $i \neq j$ that W_{ij} will be nonzero if i is being connected by j, and zero otherwise. Thus from (17), $(\mathbf{K}_1\mathbf{K}_0^{-1})_{ij}$ will be separated into two groups according to $W_{ij} = 0$ or $W_{ij} \neq 0$. By arranging the elements of $(\mathbf{K}_1\mathbf{K}_0^{-1})_{ij}$ $(i \neq j)$ in ascending order for fixed i, and employing some cluster algorithm to separate the elements into two clusters [17,18], one can identify those nodes j that connect to i. Thus one can identify the zero and nonzero W_{ij} and hence the adjacency matrix. Figure 2 displays the final results of reconstructing W_{ij} and f_i' solely using information derived from the time-series data, showing excellent agreement. Such a clustering procedure of identifying zero and nonzero W_{ij} elements can significantly enhance the reconstruction performance (see Fig. 4) and will be employed throughout in our network reconstruction scheme.

For diffusive coupling, $h' = 1$, but in practice the coupling function or h' is not known in general. In the case when h' is not known, one can still reconstruct the relative weights as

$$w_{ij} \equiv \frac{\sum_m (\mathbf{K}_1)_{im}\left(\mathbf{K}_0^{-1}\right)_{mj}}{\sum_{i\neq j}\sum_m (\mathbf{K}_1)_{im}\left(\mathbf{K}_0^{-1}\right)_{mj}} \quad \text{for } i \neq j. \tag{19}$$

Figure 3 shows the reconstruction result for a nonlinear coupling function of $h(z) = \tanh(z)$ $(h' = 1)$, $h(z) = \frac{z}{3}e^{1-\frac{|z|}{3}}$ $(h' = \frac{e}{3})$, and $h(z) = \sqrt{\frac{1}{2}}ze^{\frac{1}{2}-\frac{z^2}{2}}$ $(h' = \sqrt{\frac{e}{2}})$. In all these cases, the relative weights can be accurately reconstructed solely from the time-series data also.

The performance of our reconstruction method for random networks of various nonlinear intrinsic node dynamics and

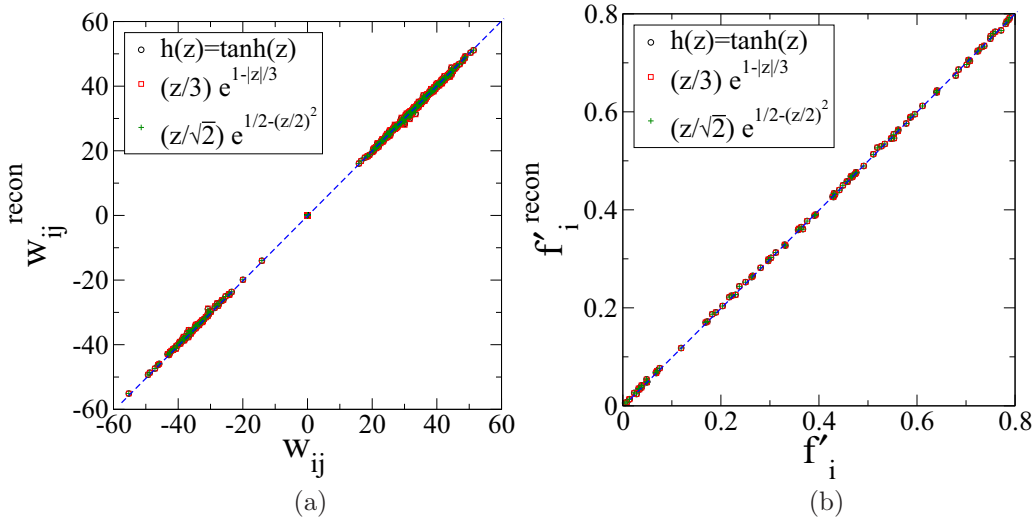

FIG. 3. Reconstruction of the directed weighted network for various nonlinear coupling functions as described in the text. Heterogeneous coupled logistic map dynamics. $T_{\rm av} = 10^6$. (a) Reconstructed relative weights using (19) vs the actual ones. (b) Reconstructed f_i' using (18) vs the actual ones.

TABLE I. Network reconstruction performance measured by the false negative and false positive error rates of the adjacency matrix, rms errors of the weight matrix (Δ_W), and derivatives of the intrinsic dynamic function f_i' ($\Delta_{f'}$) for various cases studied. Different intrinsic dynamics are considered: Heterogeneous logistic ($f_i(x) = r_i x(1-x)$ with r_i uniformly distributed in (0,0.8]), heterogeneous cubic ($f_i(x) = r_i x(1-x^2)$ with r_i uniformly distributed in (0,1]), heterogeneous Hill ($f_i(x) = r_i x^2/(1+x^2)$ with r_i uniformly distributed in (1,2]), heterogeneous Hénon map ($u_i(n+1) = 1 + v_i(n) - a_i u_i^2(n)$; $v_i(n+1) = b u_i(n)$, with $b = 0.3$ and a_i uniformly distributed in $(-0.132, -0.11]\times(1-b^2)$), and different coupling functions [$h(z)$]. Noise strength σ_{ii} is uniformly distributed in $(0, 10^{-8}]$ in all cases. WR1 are a directed weighted random network with $p = 0.05$, except for those marked with †, which are with $p = 0.07$. The four values in the column of $\Delta_{f'}$ for Hénon dynamics correspond to the rms errors of $\partial_u f_i$, $\partial_v f_i$, $\partial_u g_i$, and $\partial_v g_i$, respectively. Period-2 dynamics is denoted by (p2), and cases marked with an asterisk are reconstructed using a reconstruction scheme for periodic dynamics as described in Sec. V; the two values in the column of $\Delta_{f'}$ correspond to the rms errors of $f_i'(\langle x_i\rangle_1)$ and $f_i'(\langle x_i\rangle_2)$.

Network	Dynamics	$h(z)$	$T_{\rm av}$	$\frac{FN}{N_L}$ (%)	$\frac{FP}{N_L}$ (%)	Δ_W (%)	$\Delta_{f'}$ (%)
WR1	Logistic	z	10^6	0	0	0.025	0.262
WR1	Logistic	$\tanh(z)$	10^6	0	0	0.025	0.262
WR1	Logistic (p2)	$\tanh(2z)$	10^6	3.080	2.875	0.055	7.328
*WR1	Logistic (p2)	$\tanh(2z)$	10^6	0.205	0	0.043	0.386, 0.828
WR1	Logistic	$\frac{z}{3}e^{1-\frac{\lvert z\rvert}{3}}$	10^6	0	0	0.028	0.263
WR1	Logistic	$\sqrt{\frac{1}{2}}ze^{\frac{1}{2}-\frac{z}{2}^2}$	10^6	0	0	0.021	0.259
WR3	Logistic	z	10^6	0	0	0.025	0.253
WR1	Cubic	z	10^6	0	0	0.024	0.258
WR1	Cubic	$\tanh(z)$	10^6	0	0	0.024	0.258
WR3	Cubic	z	10^6	0	0	0.024	0.243
WR1	Hill	z	10^6	0	0.196	0.043	0.492
WR1	Hill	$\tanh(z)$	10^6	0	0.196	0.043	0.492
WR1†	Hill (p2)	z	10^6	3.212	3.491	0.763	18.30
*WR1†	Hill (p2)	z	10^6	0	0	0.048	0.508, 0.696
WR1	Hénon	z	10^6	0.204	10.43	0.389	3.639, 1.900, 0.00052, 0.761
WR1	Hénon	z	10^7	0	4.294	0.232	3.456, 0.764, 0.0009,0.358
WR1	Hénon	$\tanh(z)$	10^7	0	3.476	0.2107	3.127, 0.748, 0.0013, 0.345

coupling functions is summarized in Table I using the following quantities. Denote the number of incorrectly predicted links (nonexisting links) by FP (FN). We quantify the accuracy of the extracted network by the false positive and false negative rates as FP/N_L and FN/N_L, where N_L is the total number of links in the generated network. The root-mean-square (rms) errors of the reconstructed W_{ij} and f_i' (denoted by Δ_W and $\Delta_{f'}$, respectively) are also measured. Since for a network of given size $\Delta_{f'}$ is not sensitive to the sparsity of the connection, it serves as a good quantity to evaluate and compare the reconstruction accuracy. As shown in Table I, the reconstruction performance is in general very good, with nearly perfect reconstructed adjacency matrices except in the cases in which the noise-free dynamics does not satisfy our assumption of being in a stationary state. This issue will be discussed and handled in Sec. V. The effects of network size, noise strengths and time-series lengths, different weight distributions, and connection topologies are discussed in the following two subsections.

B. Effects of $T_{\rm av}$, network size, and noise strengths

The reconstruction formulas (17) and (18) in principle are exact if the covariance matrices $\mathbf{K}_0$ and $\mathbf{K}_1$ are computed with measurement duration $T_{\rm av} \to \infty$. But time-series data in practice are of finite length, and this will hamper the reconstruction accuracy. To investigate the effect of time-series length, the rms errors for W_{ij} and f_i' are measured for the same random network but with different $T_{\rm av}$. Figure 4 shows the rms

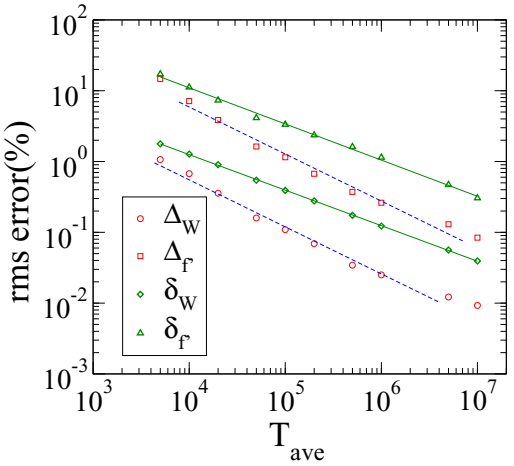

FIG. 4. Network reconstruction performance as a function of the measurement time $T_{\rm av}$. The rms errors for reconstruction of W_{ij} and f_i' using the formulas in Eqs. (17) and (18) without employing the method of clustering into connected and unconnected groups are denoted by δ_W and $\delta_{f'}$, respectively, showing the expected $1/\sqrt{T_{\rm av}}$ behaviors (solid green lines). The corresponding rms errors when W_{ij} are clustered into two groups of connected and unconnected ones are denoted by Δ_W and $\Delta_{f'}$, respectively, showing even lower rms errors (dashed blues lines). The WR1 network ($N = 100$) with heterogeneous logistic node dynamics with linear couplings distributed with two Gaussians with means 0.1 and -0.1 (with relative fractions of 0.8 and 0.2, respectively), and standard deviations 0.02.

TABLE II. Reconstruction performance for directed random networks of different sizes. p is chosen such that the mean total degree of the networks is almost the same ($\langle k\rangle \simeq 5$). Heterogeneous logistic node dynamics with linear coupling, distributed with two Gaussians with means 0.05 and −0.05 (with relative fractions of 0.8 and 0.2, respectively), and standard deviations 0.01.

N	$\langle k\rangle$	$T_{\rm av}$	$\frac{FN}{N_L}$ (%)	$\frac{FP}{N_L}$ (%)	Δ_W (%)	$\Delta_{f'}$ (%)
50	5.02	10^5	0.398	9.562	0.214	1.324
50	5.02	10^6	0.398	5.179	0.050	0.321
100	4.87	10^5	0.821	6.571	0.194	2.041
100	4.87	10^6	0	0.821	0.040	0.396
500	5.15	10^5	10.94	23.24	0.240	5.623
500	5.15	10^6	0.155	1.009	0.028	0.608
1000	5.15	10^5	16.28	19.69	0.178	7.009
1000	5.15	10^6	0.194	0.602	0.017	0.553

errors for reconstruction of W_{ij} and f_i' using the formulas in Eqs. (17) and (18) without employing the method of clustering into connected and unconnected groups (denoted by δ_W and $\delta_{f'}$, respectively) showing the expected decrease as $1/\sqrt{T_{\rm av}}$ (indicated by solid green lines with a slope of −0.5). On the other hand, when the procedure of clustering into connected and unconnected groups is used, the rms errors (denoted by Δ_W and $\Delta_{f'}$) decrease with a significantly faster rate (indicated by dashed blue lines with a slope $\simeq$0.75). For $T_{\rm av} = 10^5$, our reconstruction method is rather accurate with $\Delta_{f'} \sim$ a few %.

Next we consider the effect of network size N on the reconstruction performance. Table II lists the error rates, Δ_W and $\Delta_{f'}$, for random networks of different node numbers with approximately the same mean degree ($\simeq$5). For shorter $T_{\rm av}$, the reconstruction become less accurate for larger networks, but the difference is not prominent for longer $T_{\rm av}$. The reconstruction performance is in general rather good for $T_{\rm av} = 10^6$ $\Delta_{f'} < 1\%$ for networks of sizes up to $N = 1000$.

The reconstruction performance for different noise matrices is also evaluated and shown in Table III. Diagonal noise matrices with elements σ_{ii} uniformly distributed in some range, or with fixed noise strengths acting on the same random network, are studied. It indicates that the accuracy of reconstruction is very good and is insensitive to noises of different strengths and distributions. Remarkably, the reconstruction accuracy remains good even for extremely low noise strengths.

TABLE III. Reconstruction performance for directed random networks with $N = 100$ under different noise strengths. Heterogeneous logistic node dynamics with linear couplings distributed with two Gaussians with means 0.1 and −0.1 (with relative fractions of 0.8 and 0.2, respectively), and standard deviations 0.02. $T_{\rm av} = 10^6$.

σ_{ii}	$\frac{FN}{N_L}$ (%)	$\frac{FP}{N_L}$ (%)	Δ_W (%)	$\Delta_{f'}$ (%)
$(0,10^{-20}]$	0	0	0.0246	0.243
10^{-20}	0	0	0.0209	0.210
$(0,10^{-8}]$	0	0	0.0249	0.262
10^{-8}	0	2.659	0.0233	0.217
$(0,10^{-6}]$	0	0	0.0249	0.262
10^{-6}	0	2.659	0.0233	0.217
$(0,10^{-4}]$	0	0	0.0249	0.262
10^{-4}	0	2.659	0.0233	0.225

TABLE IV. Reconstruction performance for directed random networks with $N = 100$ under different coupling distributions. Heterogeneous logistic node dynamics linearly coupled. $P_G(\mu)$ denotes Gaussian distribution with mean μ. $P_{2G}(\alpha;\mu_1,\mu_2)$ denotes distributions with two Gaussians with means μ_1 and μ_2 (with relative fractions of α and $1-\alpha$, respectively). Gaussians are all with standard deviations of 0.02.

W distribution	$T_{\rm av}$	$\frac{FN}{N_L}$ (%)	$\frac{FP}{N_L}$ (%)	Δ_W (%)	$\Delta_{f'}$ (%)
(0.05,0.15]	10^6	0	2.464	0.0289	0.297
(−0.05,0.05]	10^6	20.33	4.928	0.0879	0.983
$P_G(0.1)$	10^6	0	0.410	0.0272	0.300
$P_G(0.02)$	10^6	29.98	4.517	0.122	1.558
$P_{2G}(0.8;0.1,-0.1)$	10^6	0	0	0.0249	0.262
$P_{2G}(0.8;0.1,0.02)$	10^6	10.06	0.205	0.093	1.148
$P_{2G}(0.8;0.1,0.02)$	10^7	4.107	0	0.0230	0.207
$P_{2G}(0.5;0.1,0.02)$	10^6	23.00	1.848	0.158	2.34
$P_{2G}(0.5;0.1,0.02)$	10^7	9.856	0	0.0534	0.770
$P_{2G}(0.2;0.1,0.02)$	10^6	33.47	2.669	0.228	4.260
$P_{2G}(0.2;0.1,0.02)$	10^7	12.32	1.027	0.0735	1.064

C. Networks of different weight distributions and connection topologies

The reconstruction performance for the same network but with different weight distributions is investigated here. We consider three types of weight distributions, namely uniformly distributed in some range, a single Gaussian, and two Gaussians with different relative proportion and their means separated. Table IV shows that the reconstruction accuracy is in general very good for different weight distributions as long as they do not cover a significant regime of very small values of weights. For very small values of weights, it can be mistaken for unconnected links and hence gives rise to high

TABLE V. Reconstruction performance for directed random networks of different connection probability p with $N = 100$. Heterogeneous logistic node dynamics with linear couplings distributed with two Gaussians with means 0.05 and −0.05 (with relative fractions of 0.8 and 0.2, respectively), and standard deviations 0.01. $N_{\rm disconn}$ denotes the number of disconnected subgraphs. $T_{\rm av} = 10^6$ except the last row is with 10^7.

p	$\langle k\rangle$	$\frac{FN}{N_L}$ (%)	$\frac{FP}{N_L}$ (%)	Δ_W (%)	$\Delta_{f'}$ (%)	$N_{\rm disconn}$
0.15	14.65	0	0	0.0464	0.422	1
0.1	9.61	0	0.104	0.0414	0.379	1
0.07	6.54	0	0.306	0.0387	0.362	1
0.05	4.87	0	0.821	0.0400	0.396	1
0.04	3.76	0	1.0634	0.0374	0.380	1
0.03	2.92	0	3.767	0.0358	0.342	5
0.02	2.05	0	12.195	0.0360	0.342	11
0.01	1.03	0	135.9	0.0605	0.568	39
0.01	1.03	0	113.6	0.0177	0.186	39

false-negative error rates. However, the errors can be reduced if $T_{\rm av}$ is increased.

The effect of network connection sparsity is examined by reconstructing random networks of different connection probabilities p. Table V shows the reconstruction performance for different sparsity. In general, the false-positive error rates increase as the network becomes more sparse, but the accuracy is still reasonably good for a rather sparse network of $p = 0.02$ (mean degree $\simeq$2 and consisting of 11 disconnected clusters). For a network that consists of many disconnected small fragments ($p = 0.01$, mean degree $\simeq$1), the reconstruction is unreliable, even if the $T_{\rm av}$ is increased (see the last row).

Finally, we evaluate the reconstruction performance for networks of different topologies but with the same size and roughly the same mean degree including small-world (SW) [26] and scale-free (SF) [4] networks. Figures 5(a)–5(d) show the predicted W_{ij} and f_i' against the actual ones for the bidirectional scale-free and small-world networks. The rewiring probability of the SW network is chosen such that the small-world characteristic is prominent. As the rewiring probability β is varied from 0 to 1, the Watt-Strogatz SW network changes from a regular network with a fixed number of degree for each node to a randomly connected network. The rms errors Δ_W and $\Delta_{f'}$ are plotted as a function of β showing some small variations in the reconstruction accuracy, but in general the reconstruction performance remains very good from regular to small-world and random networks. The reconstruction errors of the SF, SW, and random networks together with reducible networks consisting of different numbers of disconnected subnetworks of equal sizes are listed in Table VI. It appears that the reconstruction accuracies remain very good and not so sensitive to the network topologies as long as the networks remain connected. For networks consisting of more disconnected parts, the reconstruction accuracy decreases slightly.

IV. RECONSTRUCTION FOR NETWORKS OF HIGH-DIMENSIONAL INTRINSIC NODE DYNAMICS

Our reconstruction scheme can be extended for networks whose nodes are governed by high-dimensional intrinsic dynamics. Here we present an explicit reconstruction formula

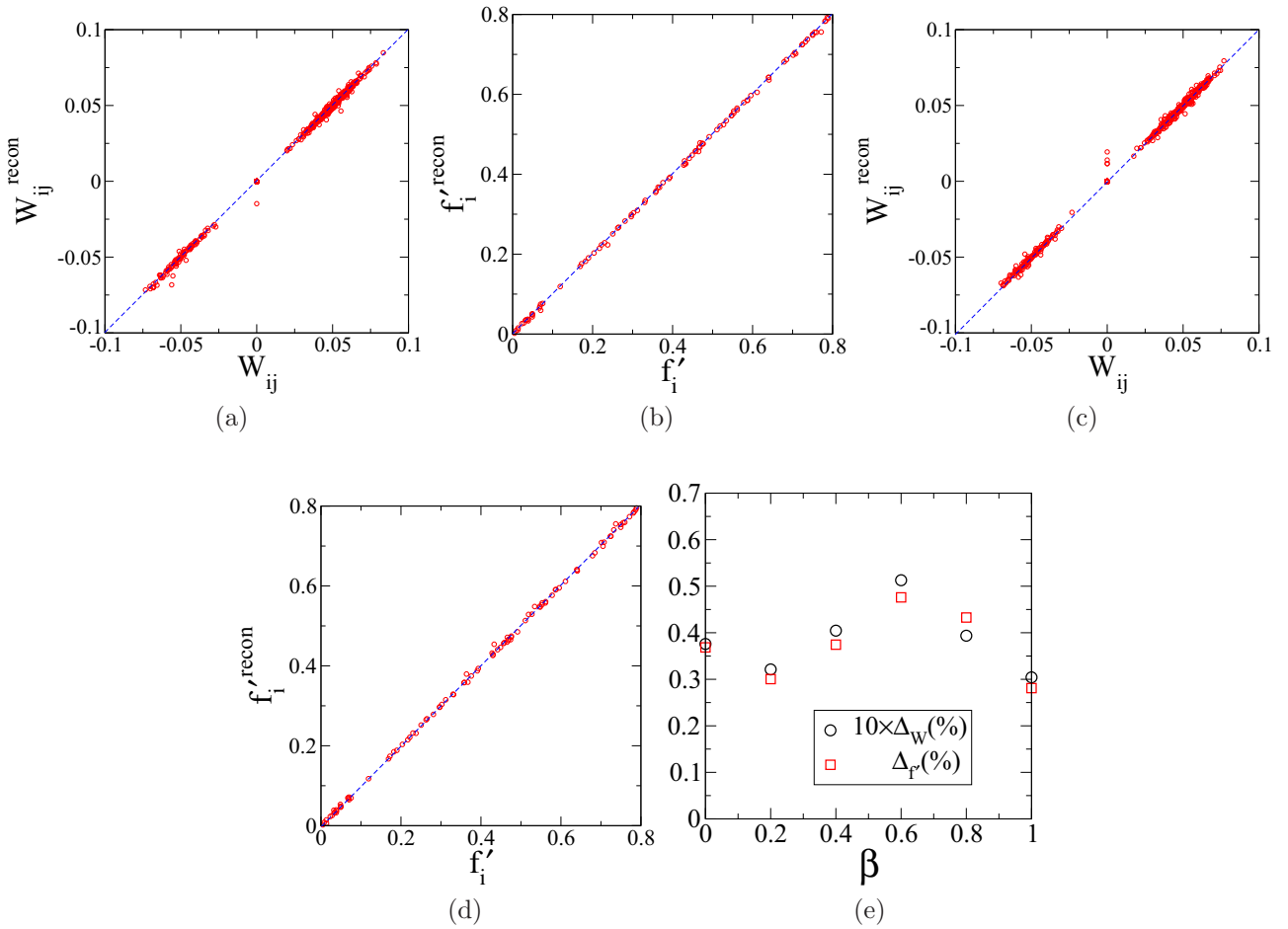

FIG. 5. Network reconstruction for networks of different topologies. $N = 100$ networks with heterogeneous logistic node dynamics with linear couplings distributed with two Gaussians with means 0.05 and -0.05 (with relative fractions of 0.8 and 0.2, respectively), and standard deviations 0.01. $T_{\rm av} = 10^6$. Scale-free bidirectional network with mean degree =5.68: (a) Reconstructed W_{ij} vs the actual W_{ij}, (b) reconstructed f_i' using vs the actual f_i'. Small-world bidirectional network with mean degree =6 and rewiring probability $\beta = 0.02$: (c) Reconstructed W_{ij} vs the actual W_{ij}, (d) reconstructed f_i' using vs the actual f_i'. (e) Reconstruction errors Δ_W and $\Delta_{f'}$ of small-world networks (mean degree =6) vs the rewiring probability β.

TABLE VI. Reconstruction performance for networks of different topologies with $N = 100$ and mean degree ∼6. Heterogeneous logistic node dynamics with linear couplings distributed with two Gaussians with means 0.05 and −0.05 (with relative fraction of 0.8 and 0.2, respectively), and standard deviations 0.01. $T_{\rm av} = 10^6$. SW: Watt-Strogatz small-world [26] bidirectional network with rewiring probability 0.02. SF: Barabási-Albert bidirectional scale-free network [4] grown with initially two nodes and adding three new nodes each time by preferential attachment. BWR: bi-directional Erdös-Rényi random network [23]. WRn: directed network with n (almost) equal-size disconnected Erdös-Rényi random subnetworks.

Network	$\langle k\rangle$	$\frac{FN}{N_L}$ (%)	$\frac{FP}{N_L}$ (%)	Δ_W (%)	$\Delta_{f'}$ (%)
SW	6	0	0.667	0.0440	0.487
SF	5.68	0	0.176	0.0365	0.368
BWR	5.92	0	0.338	0.0381	0.368
WR1	5.92	0	0.507	0.0396	0.384
WR3	5.94	0	0.673	0.0442	0.463
WR5	5.91	0	1.015	0.0436	0.433
WR10	5.96	0	1.007	0.0464	0.470

for two-dimensional dynamics, and it can be trivially extended to higher dimensions. Suppose the ith node dynamics is described by $u_i(n)$ and $v_i(n)$ and coupled only via u in the network. The dynamics of the network system is described by

$$u_i(n+1) = f_i(u_i(n), v_i(n)) + \sum_j W_{ij} h(u_i(n), u_j(n)) + \eta_i^u(n), \tag{20}$$

$$v_i(n+1) = g_i(u_i(n), v_i(n)) + \eta_i^v(n), \tag{21}$$

where η_i^u and η_i^v are independent zero-mean white noises acting on the dynamical variables, and f_i and g_i are functions governing the intrinsic two-dimensional node dynamics. Again consider small deviations from the noise-free steady-state solution $(u_i(n), v_i(n)) = (U_i, V_i)$, $y_i(n) \equiv u_i(n) - U_i$, and $z_i(n) \equiv v_i(n) - V_i$. Then upon linearizing about the noise-free solution, one has

$$\vec{\zeta}(n+1) = \mathbf{M}\vec{\zeta}(n) + \vec{\eta}(n), \tag{22}$$

where $\vec{\zeta} \equiv (\vec{y}, \vec{z})$ and $\vec{\eta} \equiv (\vec{\eta}^u, \vec{\eta}^v)$ are vectors of length $2N$, and $\mathbf{M}$ is the $2N \times 2N$ matrix

$$\mathbf{M} \equiv \begin{bmatrix} \mathbf{N} & \partial_{\mathbf{v}}\mathbf{f} \\ \partial_{\mathbf{u}}\mathbf{g} & \partial_{\mathbf{v}}\mathbf{g} \end{bmatrix}, \tag{23}$$

and the $N \times N$ matrices are given by

$$\mathbf{N}_{ij} = W_{ij}\partial_2 h(U_i, U_j) + \left[\sum_m W_{im}\partial_1 h(U_i, U_m) + \partial_u f_i(U_i, V_i)\right]\delta_{ij}, \tag{24}$$

$$(\partial_{\mathbf{v}}\mathbf{f})_{ij} = \partial_v f_i(U_i, V_i)\delta_{ij}, \tag{25}$$

$$(\partial_{\mathbf{u}}\mathbf{g})_{ij} = \partial_u g_i(U_i, V_i)\delta_{ij}, \tag{26}$$

$$(\partial_{\mathbf{v}}\mathbf{g})_{ij} = \partial_v g_i(U_i, V_i)\delta_{ij}. \tag{27}$$

Following similar procedures as in the previous section, one computes the $2N \times 2N$ covariance matrices $\mathbf{K}_0 \equiv \langle\vec{\zeta}(n)\vec{\zeta}^{\mathsf{T}}(n)\rangle$ and $\mathbf{K}_\tau \equiv \langle\vec{\zeta}(n+\tau)\vec{\zeta}^{\mathsf{T}}(n)\rangle$. The matrices $\mathbf{M}$ and $\boldsymbol{\sigma} \equiv \langle\vec{\zeta}(n)\vec{\zeta}^{\mathsf{T}}(n)\rangle$ can be extracted as

$$\mathbf{M} = \mathbf{K}_1\mathbf{K}_0^{-1} = \mathbf{K}_2\mathbf{K}_1^{-1} = \cdots \mathbf{K}_\tau\mathbf{K}_{\tau-1}^{-1}, \tag{28}$$

$$\boldsymbol{\sigma} = \mathbf{K}_0 - \mathbf{M}\mathbf{K}_0\mathbf{M}^{\mathsf{T}} = \mathbf{K}_0 - \mathbf{K}_1\mathbf{K}_0^{-1}\mathbf{K}_1^{\mathsf{T}}. \tag{29}$$

From the extracted $\mathbf{M}$, one can obtain N_{ij} and the partial derivatives $\partial_v f_i$, $\partial_u g_i$, and $\partial_v g_i$ from (23). W_{ij} and $\partial_u f_i$ can then be reconstructed via

$$N_{ij} = W_{ij}\partial_2 h(U_i, U_j), \quad i \neq j, \tag{30}$$

$$N_{ii} = \partial_u f_i(U_i, V_i) + \sum_m W_{im}\partial_1 h(U_i, U_m). \tag{31}$$

Here we demonstrate our method using the two-dimensional Hénon map [27] linearly coupled in a network with $\partial_2 h = 1 = -\partial_1 h$. The intrinsic dynamics of each (inhomogeneous) node is described by

$$f_i(u_i, v_i) = 1 + v_i - a_i u_i^2, \tag{32}$$

$$g_i(u_i, v_i) = b u_i^2, \tag{33}$$

with $\partial_u f_i = -2a_i U_i$, $\partial_v f_i = 1$, $\partial_v g_i = 0$, and $\partial_u g_i = b$. The (known) matrix $\mathbf{M}$ is simply

$$\mathbf{M} = \begin{bmatrix} \mathbf{N} & \mathbf{I} \\ b\mathbf{I} & \mathbf{0} \end{bmatrix}, \quad N_{ij} = W_{ij} \quad (i \neq j),$$
$$N_{ii} = -2a_i U_i - \sum_m W_{im}. \tag{34}$$

Figure 6(a) is a plot of the matrix elements of $\mathbf{K}_1\mathbf{K}_0^{-1}$ versus the corresponding known elements of $\mathbf{M}$ given in Eq. (34), verifying the reconstruction formula (28). Figures 6(b) and 6(c) display the reconstruction results of W_{ij},σ_{ii} using only the time-series data, exhibiting high accuracy. Figure 6(d) plots the reconstructed partial derivatives of f and g against their known values, again showing good agreement. The last three rows of Table I show that the reconstruction performance of the Hénon map network is in general good, although a long $T_{\rm av} = 10^7$ is needed to achieve the same level of accuracy for the other cases of 1D intrinsic node dynamics. Note that there are four rms errors for $\Delta_{f'}$ in Table I corresponding to the partial derivatives $\partial_u f_i$, $\partial_v f_i$, $\partial_u g_i$, and $\partial_v g_i$, respectively.

V. RECONSTRUCTION FOR NETWORKS WITH PERIODIC DYNAMICS

In the previous sections, the noise-free dynamics was assumed to be stationary, and the node dynamics $x_i(n)$ fluctuates around the time-independent X_i. In coupled map networks, even though the uncoupled dynamics of each node is stationary, coupling can easily induce the system to undergo period doubling bifurcations [28,29] to periodic states and even to chaotic dynamics. Here we allow for the situation in which the noise-free dynamics $X_i(n)$ is periodic, and we derive the network reconstruction formulas when the nodes are under white noises. Explicit demonstrations are shown for period-2

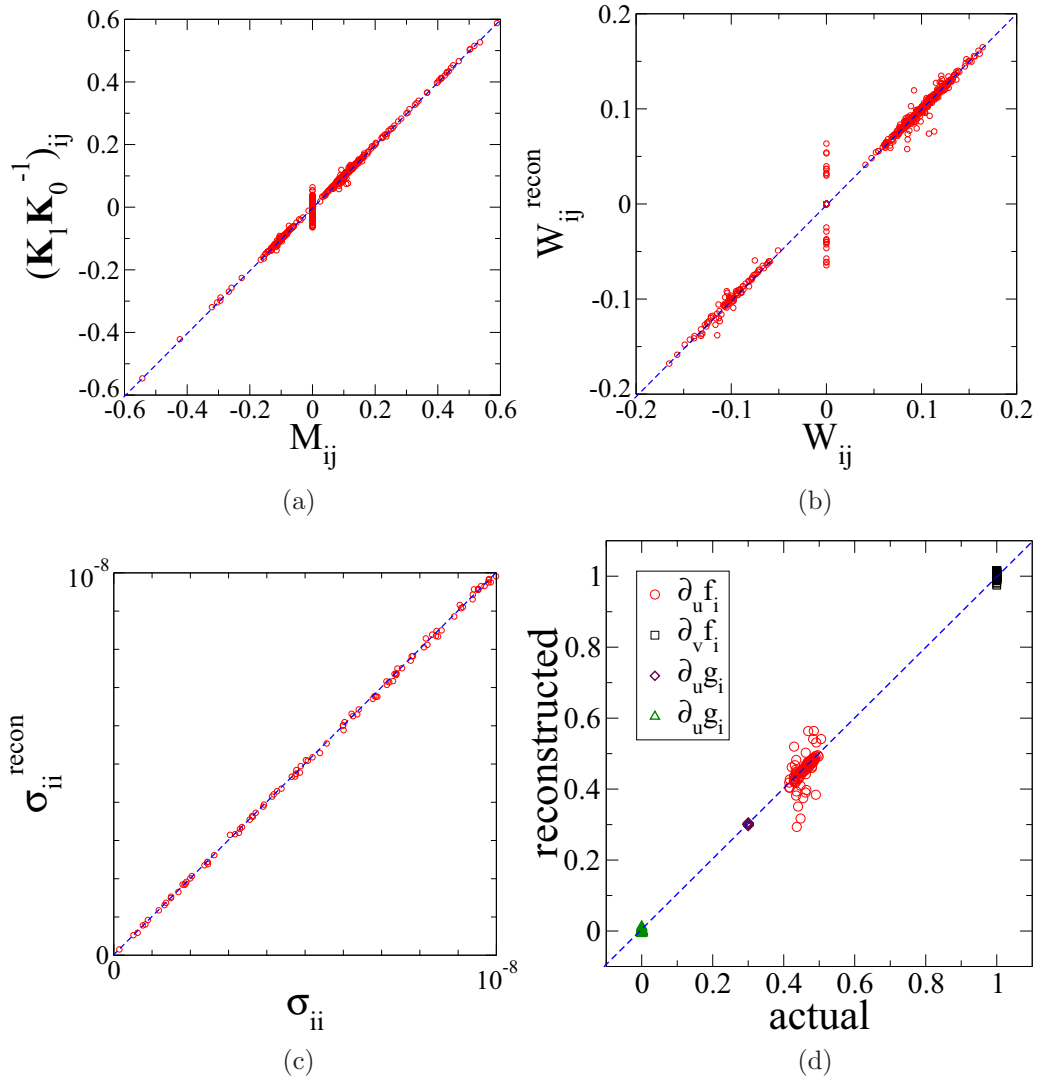

FIG. 6. Reconstruction of the directed weighted network with intrinsic node dynamics given by the heterogeneous Hénon map: $u_i(n+1) = 1 + v_i(n) - a_i u_i^2$, $v_i(n+1) = b u_i(n)$ with $b = 0.3$ and a_i uniformly distributed in $(-0.132, -0.11]\times(1-b^2)$, and linear couplings. $T_{\rm av} = 10^7$. (a) $(\mathbf{K}_1\mathbf{K}_0^{-1})_{ij}$ vs the actual M_{ij}, verifying the reconstruction formula (28). (b) The reconstructed W_{ij} using (24) vs the actual W_{ij}. (c) The reconstructed σ_{ii} using (29) vs the actual σ_{ii}. (d) The reconstructed partial derivative matrix elements using (23) and (28) vs the actual ones.

network dynamics for two cases, as shown in Table I (marked with asterisks).

Suppose the noise-free solution of the network dynamics is synchronized with period P. Again consider small deviations from the noise-free periodic solution $X_i(n)$, $y_i(n) \equiv x_i(n) - X_i(n)$. Expanding to linear order, one gets

$$\vec{y}(n+1) \simeq \mathscr{N}\vec{y}(n) + \mathbf{F}\vec{y}(n) + \vec{\eta}(n), \tag{35}$$

where $\mathbf{F}$ is the diagonal matrix with diagonal elements $f_i'(X_i(n))$, and $\mathscr{N}_{ij} \equiv h'(W_{ij} - \delta_{ij}\sum_m W_{im})$. Note that we have separated the time-dependent part $\mathbf{F}$, and $\mathscr{N}$ is time-independent. To derive the reconstruction formulas, again we need to compute the covariance matrices $\mathbf{K}_0$ and $\mathbf{K}_1$. The key idea is that even though the asymptotic dynamics fluctuates around the periodic orbit consisting of P points, labeled as $X_i^{(1)}, \ldots, X_i^{(P)}$, all time averages of the fluctuating quantities can be decomposed into a sum of averages around the $X_i^{(k)}$'s ($k = 1, \ldots, P$) as

$$P\langle\cdots\rangle = \langle\cdots\rangle_1 + \langle\cdots\rangle_2 + \cdots\langle\cdots\rangle_P, \tag{36}$$

where $\langle\cdots\rangle_k$ denotes averages taken from (after the transient times and the system undergoes its asymptotic periodic dynamics) time point $k, k+P, k+2P, \ldots$. Since these time points are separated by the period P, values of x_i measured at these time points fluctuate around the noise-free point $X_i^{(k)}$. Furthermore, in practice the noise-free periodic orbit can be obtained from the time-series data via

$$X_i^{(k)} \simeq \langle x_i\rangle_k, \quad k = 1, \ldots, P. \tag{37}$$

Figure 7(a) shows the measured $\langle x_i\rangle_k$ versus the corresponding noise-free $X_i^{(k)}$ for the period-2 dynamics generated by intrinsic Hill dynamics and linear coupling (see Table I), verifying the validity of (37).

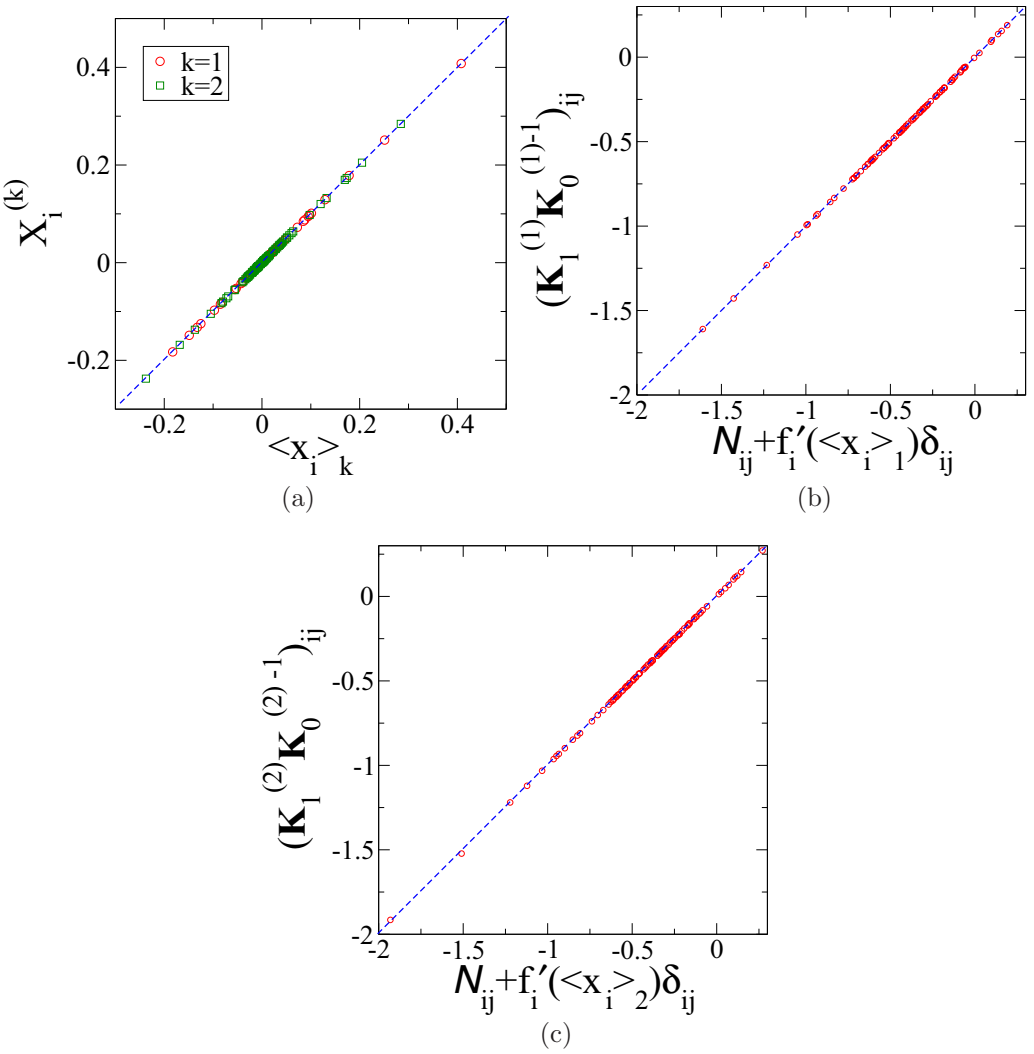

FIG. 7. Verification of the reconstruction formulas for the directed weighted network having period-2 noise-free dynamics. Heterogeneous coupled Hill map dynamics and linear couplings. $T_{\rm av} = 10^6$. (a) The noise-free periodic point $X_i^{(k)}$ vs $\langle x_i \rangle_k$, verifying (37). (b) $(\mathbf{K}_1^{(1)}\mathbf{K}_0^{(1)^{-1}})_{ij}$ vs the actual $\mathcal{N}_{ij} + f_i'(\langle x_i \rangle_1)\delta_{ij}$, verifying (45) for $k = 1$. (c) $(\mathbf{K}_1^{(2)}\mathbf{K}_0^{(2)^{-1}})_{ij}$ vs the actual $\mathcal{N}_{ij} + f_i'(\langle x_i \rangle_2)\delta_{ij}$, verifying (45) for $k = 2$.

Now we compute the periodically averaged time-lagged covariance matrix defined as

$$\mathbf{K}_1^{(k)} = \langle \vec{y}(n+1)\vec{y}^{\intercal}(n)\rangle_k, \quad k = 1,2,\ldots,P, \tag{38}$$

$$= \mathcal{N}\langle \vec{y}(n)\vec{y}^{\intercal}(n)\rangle_k + \langle \mathbf{F}\vec{y}(n)\vec{y}^{\intercal}(n)\rangle_k, \tag{39}$$

$$\simeq (\mathcal{N} + \mathbf{F}^{(k)})\mathbf{K}_0^{(k)}, \quad \mathbf{F}_{ij}^{(k)} \equiv f_i'(\langle x_i \rangle_k)\delta_{ij}. \tag{40}$$

Similarly, one computes

$$\begin{aligned}\mathbf{K}_0^{(k)} &= \langle \vec{y}(n)\vec{y}^{\intercal}(n)\rangle_k \\ &= \langle \mathcal{N}\vec{y}(n)\vec{y}^{\intercal}(n)\mathcal{N}^{\intercal}\rangle_k + \langle \mathcal{N}\vec{y}(n)\vec{y}^{\intercal}(n)\mathbf{F}\rangle_k \\ &\quad + \langle \mathbf{F}\vec{y}(n)\vec{y}^{\intercal}(n)\mathcal{N}^{\intercal}\rangle_k + \langle \vec{\eta}(n)\vec{\eta}^{\intercal}(n)\rangle_k + \mathscr{M}^{(k)} \\ &= \mathcal{N}\mathbf{K}_0^{(k)}\mathcal{N}^{\intercal} + \mathcal{N}\mathbf{K}_0^{(k)}\mathbf{F}^{(k)} + \mathbf{F}^{(k)}\mathbf{K}_0^{(k)}\mathcal{N}^{\intercal} + \boldsymbol{\sigma} + \mathscr{M}^{(k)},\end{aligned} \tag{41}$$

where

$$\mathscr{M}_{ij}^{(k)} \equiv \langle f_i'(X_i(n)) f_j'(X_j(n)) y_i(n) y_j(n)\rangle_k \tag{42}$$

$$\simeq f_i'(\langle x_i \rangle_k) f_j'(\langle x_i \rangle_k) K_{0\ ij}^{(k)}. \tag{43}$$

Using (40) to eliminate $\mathbf{F}^{(k)}\mathbf{K}_0^{(k)}$, one gets

$$\mathbf{K}_0^{(k)} = -\mathcal{N}\mathbf{K}_0^{(k)}\mathcal{N}^{\intercal} + \mathbf{K}_1^{(k)}\mathcal{N}^{\intercal} + \mathcal{N}\mathbf{K}_1^{(k)^{\intercal}} + \boldsymbol{\sigma} + \mathscr{M}^{(k)}. \tag{44}$$

Thus $\mathcal{N}$ can be reconstructed from the off-diagonal and diagonal elements of $\mathbf{K}_1^{(k)}\mathbf{K}_0^{(k)^{-1}}$ via

$$\mathbf{K}_1^{(k)}\mathbf{K}_0^{(k)^{-1}} = \mathcal{N} + \mathbf{F}^{(k)}, \quad k = 1,\ldots,P. \tag{45}$$

Hence the reconstruction formulas for the $\mathbf{W}$ and $f_i'(\langle x_i \rangle_k)$ are

$$h' W_{ij} = \left(\mathbf{K}_1^{(k)}\mathbf{K}_0^{(k)^{-1}}\right)_{ij} \quad \text{for} \quad i \neq j, \quad W_{ii} = 0, \tag{46}$$

$$f_i'(\langle x_i \rangle_k) = \sum_{m \neq i} \left(\mathbf{K}_1^{(k)}\mathbf{K}_0^{(k)^{-1}}\right)_{im} + \left(\mathbf{K}_1^{(k)}\mathbf{K}_0^{(k)^{-1}}\right)_{ii}. \tag{47}$$

Then $\boldsymbol{\sigma}$ can be reconstructed from (44) once $\mathcal{N}$ and the $f_i'(\langle x_i \rangle_k)$'s are known.

To verify our reconstruction scheme for periodic dynamics, period-2 noise-free dynamics is generated using a similar random network with intrinsic Hill dynamics but with a

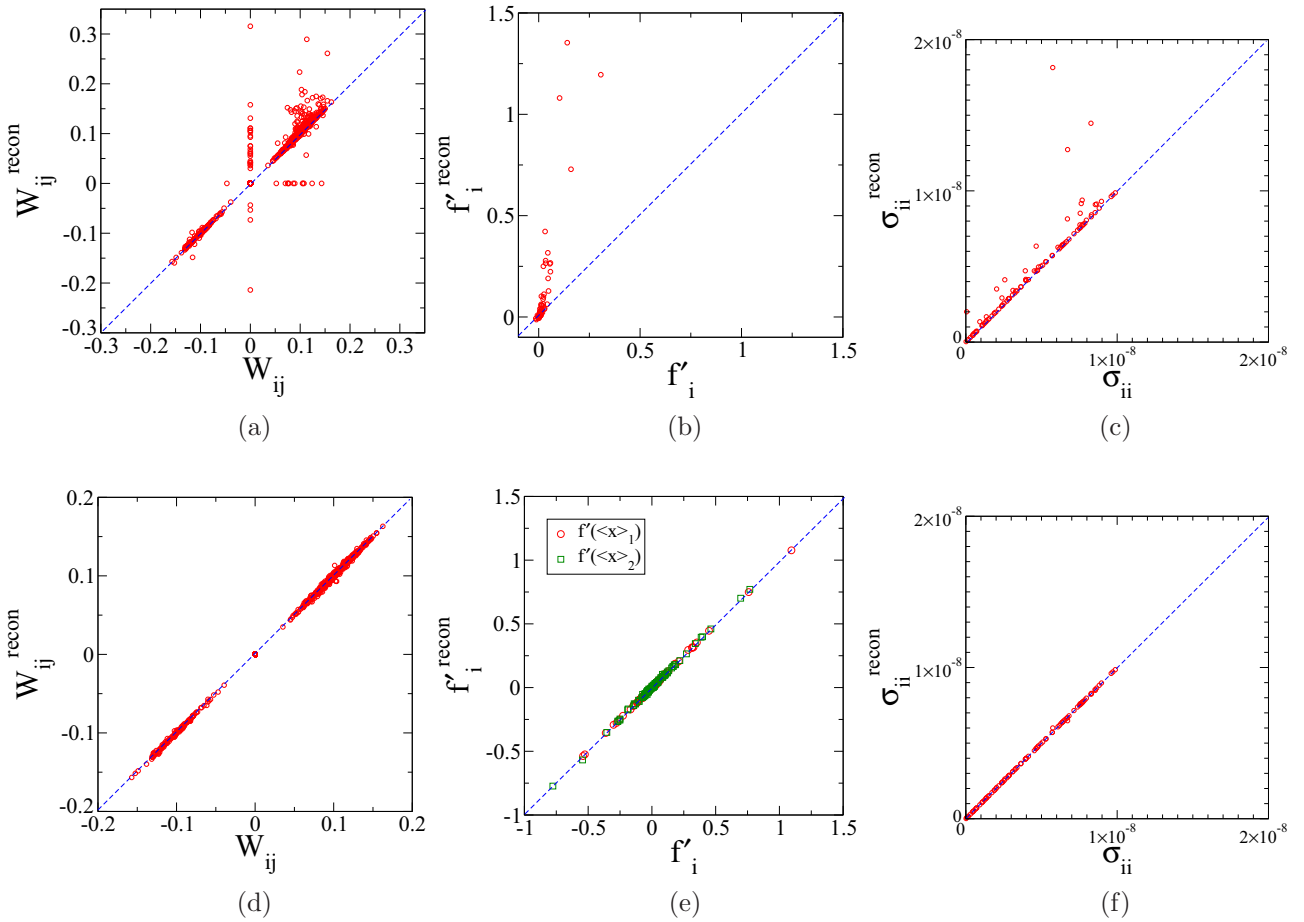

FIG. 8. Network reconstruction for period-2 noise-free dynamics for the same system in Fig. 7. (a) Naive use of the reconstruction formula for stationary noise-free dynamics in reconstructing W_{ij} using (17). (b) Naive use of the reconstruction formula for stationary noise-free dynamics in reconstructing f_i' using (18). (c) Naive use of the reconstruction formula for stationary noise-free dynamics σ_{ii} using (15). (d) Reconstructed W_{ij} using (46) for periodic dynamics vs the actual W_{ij}. (e) The reconstructed partial derivative matrix elements using (47) for periodic dynamics vs the actual ones. (f) The reconstructed σ_{ii} using (44) for periodic dynamics vs the actual σ_{ii}.

higher connection probability of $p = 0.07$ (WR1† in Table I); the resultant dynamics is period-2 due to the higher link density in the network. Figures 7(b) and 7(c) verify that the reconstruction formulas in Eq. (45) for period-2 dynamics indeed hold very well.

On the other hand, if one naively applies the reconstruction method for stationary dynamics to this case of period-2 dynamics, the error rates for the adjacency matrix are $FN/N_L = 3.21\%$ and $FP/N_L = 3.49\%$ and the rms errors are large, with $\Delta_W = 0.76\%$, $\Delta_{f'} = 18.3\%$ (see Table I). On the other hand, when the correct method of reconstructing period-2 dynamics is used, one gets perfect reconstruction of the adjacency matrix and the rms errors drop significantly to $\Delta_W = 0.048\%$, $\Delta_{f'}$'s $= 0.508\%$ and 0.696%, indicating the validity of the reconstruction method for fluctuating periodic dynamics in a network. Figure 8 shows the comparison of reconstruction results (for W_{ij}, f_i', and σ_{ii}) when one naively applies a reconstruction scheme for stationary dynamics to that of the correct reconstruction formulas for periodic dynamics. Many false-positive and false-negative connections are incorrectly reconstructed unless the correct reconstruction formulas are used. Furthermore, the predictions for f_i' deviate enormously if the correct reconstruction scheme for periodic dynamics is not employed. In addition to the period-2 state generated with Hill dynamics, our method also works well for the period-2 state generated for WR of $p = 0.05$ with logistic node dynamics with the coupling function $h(z) = \tanh(2z)$. As shown in Table I, very accurate network reconstruction can be achieved with the proper reconstruction scheme for period-2 dynamics.

VI. CONCLUSION AND OUTLOOK

In this paper, we derived analytic formulas for reconstructing the connection strengths and topology of directed network systems with discrete-time dynamics under white noises. The derived reconstruction formulas (14)–(16) provide the theoretical basis for our network reconstruction scheme. Only time-series data of the measured nodal dynamics are required as input for the network reconstruction. Information about the intrinsic node dynamics as well as the noise strengths can also be obtained. All the reconstruction schemes are well verified by numerically generated time-series data of weighted directed and undirected networks of known connection and coupling strengths. The performance of the network reconstruction is evaluated in terms of false positive

and false negative error rates together with the rms errors for W_{ij} and f_i' for various parameters, including the time-series length $T_{\rm av}$, the network size N, the noise matrix σ_{ij}, the weight distribution, the network sparsity, and different network topologies such as small-world, scale-free, and reducible block networks. Our results indicated that our reconstruction scheme in general is accurate for a broad range of parameters and network topologies. Only for cases when the network is very fragmented or when the coupling weights contain a significant portion of very small weights is the accuracy less satisfactory. In addition, we also go beyond previous network reconstruction methods of continuous-time dynamics [17–19], and we derive reconstruction formulas [Eqs. (28)–(31)] for higher-dimensional node dynamics as well as for situations when the noise-free dynamics is periodic [Eqs. (44)–(47)]. The reconstruction method for period states presented here considered the entire network with all nodes having the same periodicity. Our scheme can be generalized to situations when the network consists of several clusters of periodic states with different periodicities; those results will be published elsewhere. Our approach for situations of high-dimensional node dynamics and a periodic noise-free state can be extended to the case of a continuous-time dynamics network governed by ordinary differential equations.

Our reconstruction method relies on fluctuations about a unique stationary dynamical state that is constantly perturbed by noises. However, multiple stable fixed points for noise-free dynamics may coexist in some scenarios, and for large measurement duration the system can hop from one stationary state to another due to noises, which might cause inaccurate network reconstruction. The present reconstruction scheme can still work in principle with the following data preprocessing procedure, provided the noisy fluctuations about different stationary states are still separated under noisy perturbations. First identify the coexisting stationary states by examining the time series. The transition between different stationary states can be identified by large hops. Then identify and collect time-series segments for the fluctuating dynamics (discarding the short transient parts just before and after transitions) around a certain stationary state, and perform reconstruction for such a collection of time-series data. Repeat the above procedure for other coexisting stationary states. One can cross-check the reconstructed networks obtained from different coexisting stationary states for consistency and possibly to improve the network prediction accuracy.

Noise is regarded as intrinsic in our system, and not externally imposed or controllable. The present work considered only nodes under additive white noises, but there are temporal correlated color noises in many practical situations. In general, there might be some node dynamics that are hidden (not available for measurements), and this would induce correlations in the effective noises felt by the measured nodes. Hence, it would be necessary to consider correlated noises. Table VII shows the performance of a naive use of the present white noise reconstruction scheme; it can only give satisfactory results if the noise correlation time $\tau_c \lesssim 0.4$ for the WR1 network used in Table I. On the other hand, our reconstruction scheme can be extended to the case of correlated color noises. The challenge would be to extract τ_c at the same time; these results will be presented elsewhere [30]. For the case of multiplicative noises in which the noise strength depends on the dynamical variable, for instance the noise term in Eq. (1) is given by $\gamma(x_i(n))\eta_i(n)$ for some function $\gamma(x)$, the present reconstruction scheme still works well. Because of the discrete-time nature of the dynamics, the reconstruction formulas (14) and (15) still hold for multiplicative noises with σ_{ij} replaced by $\gamma(X_i)\gamma(X_j)\sigma_{ij}$, hence W_{ij} and f_i' can be reconstructed accurately using the same scheme.

TABLE VII. Reconstruction performance for a directed weighted random network under correlated noises with correlation time τ_c. Logistic dynamics and linear coupling the same as the network in the first row of Table I. $T_{\rm av} = 10^6$.

τ_c	$\frac{FN}{N_L}$ (%)	$\frac{FP}{N_L}$ (%)	Δ_W (%)	$\Delta_{f'}$ (%)
0	0	0	0.025	0.262
0.2	0	0	0.032	0.649
0.4	0	2.316	0.148	6.382
0.6	0	9.895	0.411	14.29
0.8	0	11.79	0.623	21.11
1.0	0	17.05	0.809	26.27

Finally, we remark that accurate and efficient network reconstruction methods developed in this work can have broad potential applications. For example, novel tools for data analysis with real-time information about the coupling strengths of the complex interacting systems may be able to provide revolutionary tools for a real-time feedback control method in science and engineering. Knowing the network interactions and their strengths, a feedback control method [31–34] can be designed and implemented to manipulate the system to the desired dynamical states across the network, with possible applications to control the dynamical state of neuronal or brain networks, or to control gene expressions in cell development.

ACKNOWLEDGMENT

This work has been supported by the Ministry of Science and Technology of Taiwan under Grant No. MOST103-2112-M-008-003-MY3, and NCTS of Taiwan.

[1] Nature, Special issue on Big Data **455** (2008).
[2] M. Timme and J. Casadiego, J. Phys. A **47**, 343001 (2014).
[3] D. Marbach *et al.*, Nat. Meth. **9**, 796 (2012).
[4] R. Albert and A.-L. Barabási, Rev. Mod. Phys. **74**, 47 (2002).
[5] S. H. Strogatz, Nature (London) **410**, 268 (2001).
[6] M. E. J. Newman, SIAM Rev. **45**, 167 (2003).
[7] J. M. Stuart, E. Segal, D. Killer, and S. K. Jim, Science **302**, 249 (2003).
[8] F. Emmert-Streib, G. V. Glazko, G. Altay, and R.de Matos Simoes, Front. Gen. **3**, 1 (2012).
[9] V. M. Eguiluz, D. R. Chialvo, G. A. Cecchi, M. Baliki, and A. V. Apkarian, Phys. Rev. Lett. **94**, 018102 (2005).

[10] M. Timme, Europhys. Lett. **76**, 367 (2006).
[11] L. Lü and T. Zhou, Physica A **390**, 1150 (2011).
[12] D. Yu, M. Righero, and L. Kocarev, Phys. Rev. Lett. **97**, 188701 (2006).
[13] M. Timme, Phys. Rev. Lett. **98**, 224101 (2007).
[14] S. G. Shandilya and M. Timme, New J. Phys. **13**, 013004 (2011).
[15] Z. Levnajic and A. Pikovsky, Phys. Rev. Lett. **107**, 034101 (2011).
[16] Z. Levnajic and A. Pikovsky, Sci. Rep. **4**, 5030 (2014).
[17] E. S. C. Ching, P. Y. Lai, and C. Y. Leung, Phys. Rev. E **88**, 042817 (2013).
[18] E. S. C. Ching, P. Y. Lai, and C. Y. Leung, Phys. Rev. E **91**, 030801(R) (2015).
[19] E. S. C. Ching and H. C. Tam, Phys. Rev. E **95**, 010301(R) (2017).
[20] Z. Zhang, Z. Zheng, H. Niu, Y. Mi, S. Wu, and G. Hu, Phys. Rev. E **91**, 012814 (2015).
[21] K. Kaneko, Chaos **2**, 279 (1992).
[22] J. Ren, W.-X. Wang, B. Li, and Y.-C. Lai, Phys. Rev. Lett. **104**, 058701 (2010).
[23] P. Erdös and A. Rényi, Publ. Math. Inst. Hung. Acad. Sci. **5**, 17 (1960).
[24] B. Bollobás, *Random Graphs* (Academic Press, London, 1985).
[25] R. M. May, Nature (London) **261**, 459 (1976).
[26] D. J. Watts and S. H. Strogatz, Nature (London) **393**, 440 (1998).
[27] M. Hénon, Commun. Math. Phys. **50**, 69 (1976).
[28] S. H. Strogatz, *Nonlinear Dynamics and Chaos*, 2nd ed. (Westview, Cambridge, 2014).
[29] H. G. Schuster and J. Wolfram, *Deterministic Chaos, An Introduction*, 4th ed. (Wiley-VCH, Weinheim, 2005).
[30] P. Y. Lai (unpublished).
[31] *Handbook of Chaos Control*, 2nd ed., edited by E. Scholl and H. G. Schuster (Wiley-VCH, Weinheim, 2008).
[32] S. Sridhar, D. M. Le, Y. C. Mi, S. Sinha, P. Y. Lai, and C. K. Chan, Phys. Rev. E **87**, 042712 (2013).
[33] S. N. Liang, D. M. Le, P. Y. Lai, and C. K. Chan, Euorphys. Lett. **115**, 48001 (2016).
[34] D. M. Le, Y. T. Lin, Y. H. Yang, P. Y. Lai, and C. K. Chan, Europhys. Lett. (to be published).